



HAL
open science

Electronic Band Structure and Transport Properties of the Cluster Compound $\text{Ag}_3\text{Tl}_2\text{Mo}_{15}\text{Se}_{19}$

Patrick Gougeon, Philippe Gall, Rabih Al Rahal Al Orabi, Benoît Boucher,
Bruno Fontaine, Regis Gautier, Anne Dauscher, Christophe Candolfi,
Bertrand Lenoir

► **To cite this version:**

Patrick Gougeon, Philippe Gall, Rabih Al Rahal Al Orabi, Benoît Boucher, Bruno Fontaine, et al..
Electronic Band Structure and Transport Properties of the Cluster Compound $\text{Ag}_3\text{Tl}_2\text{Mo}_{15}\text{Se}_{19}$.
Inorganic Chemistry, 2019, 58 (9), pp.5533-5542. 10.1021/acs.inorgchem.8b03452 . hal-02120748

HAL Id: hal-02120748

<https://univ-rennes.hal.science/hal-02120748>

Submitted on 20 Mar 2020

HAL is a multi-disciplinary open access archive for the deposit and dissemination of scientific research documents, whether they are published or not. The documents may come from teaching and research institutions in France or abroad, or from public or private research centers.

L'archive ouverte pluridisciplinaire **HAL**, est destinée au dépôt et à la diffusion de documents scientifiques de niveau recherche, publiés ou non, émanant des établissements d'enseignement et de recherche français ou étrangers, des laboratoires publics ou privés.

Electronic Band Structure and Transport Properties of the Cluster Compound



Patrick Gougeon^{1*}, Philippe Gall¹, Rabih Al Rahal Al Orabi^{1,§*}, Benoit Boucher¹,
Bruno Fontaine¹, Régis Gautier¹, Anne Dauscher², Christophe Candolfi², Bertrand Lenoir²

¹*Univ Rennes, INSA-ENSCR, CNRS, ISCR-UMR 6226,
F-35000 Rennes, France.*

²*Institut Jean Lamour, UMR 7198 CNRS – Université de Lorraine, 2 allée André Guinier-
Campus ARTEM, BP 50840, 54011 Nancy Cedex, France*

§ Present addresses: (a) Solvay, Design and Development of Functional Materials Department, Axel'One, 69192 Saint Fons, France and (b) Central Michigan University, Department of Physics, Mt. Pleasant, MI 48859, USA.

Abstract

Mo-based cluster compounds are a large class of materials with complex crystal structures that give rise to very low lattice thermal conductivity. Here, we report on the crystal structure and transport properties measurements (5 – 800 K) of the novel Tl-filled compound $\text{Ag}_3\text{Tl}_2\text{Mo}_{15}\text{Se}_{19}$. This compound adopts a crystal structure described in the rhombohedral $R\bar{3}c$ space group ($a = 9.9601(1)$ Å, $c = 57.3025(8)$ Å, and $Z = 6$) built by a covalent arrangement of octahedral Mo_6 and bioctahedral Mo_9 clusters in a 1:1 ratio with the Ag and Tl atoms filling the large cavities between them. Transport properties measurements performed on polycrystalline samples indicate that this compound behaves as a heavily-doped semiconductor with mixed electrical conduction. Electronic band structure calculations

combined with a semi-classical approach using the Boltzmann transport equation are in good agreement with these measurements. This compound exhibits a lattice thermal conductivity as low as $0.4 \text{ W m}^{-1} \text{ K}^{-1}$ due to highly disordered Ag and Tl atoms. Because of the low thermopower values induced by the mixed electrical conduction, the dimensionless thermoelectric figure of merit ZT remains moderate with a peak value of 0.2 achieved at 800 K.

Accepted manuscript

Introduction

Solid-state thermoelectric generators and refrigerators are robust and scalable devices that enable to convert waste heat into electricity and an electrical current into a thermal gradient, respectively.¹⁻³ However, their efficiency, determined by the dimensionless thermoelectric figure of merit $ZT = \alpha^2 T / \rho \kappa$ where α is the thermopower, T is the absolute temperature, ρ is the electrical resistivity and κ is the total thermal conductivity, needs to be further improved to make them competitive with other green-energy technologies.¹⁻³ This simple formula encompasses the inherent difficulties encountered in the optimization of the thermoelectric properties of semiconductors. A good thermoelectric material should indeed strike a delicate balance between a large thermopower, a low electrical resistivity and a low total thermal conductivity. In non-magnetic compounds, κ is composed of an electronic contribution κ_e and a lattice contribution κ_L . Except for κ_L , all the other transport coefficients are interdependent via the carrier concentration. One possible strategy is thus to seek materials in which the phonon conduction is naturally glass-like, that is, materials that exhibit phonon mean free paths on the order of the mean interatomic distance.

Compounds composed of a covalent network of Mo- Q clusters ($Q = S, Se$ or Te) represent a large class of materials in which several electronic or magnetic phenomena have been identified.⁴⁻¹⁰ Thanks to their rich chemistry and inherently glass-like thermal conductivity, they represent an interesting platform for designing novel thermoelectric materials.¹¹⁻¹⁹ These compounds are made up of cluster units, the size and geometry of which can vary appreciably from Mo_3 up to Mo_{36} .⁴⁻¹⁰ The arrangement of these clusters in the unit cell leaves large channels or cavities where various cations (alkali, alkaline-earth, rare-earth or transition metals) can reside.⁴⁻¹⁹ Although the crystal structure of many of these compounds was reported in the 1980s, it is not until recently that their thermoelectric properties have been assessed.¹¹⁻¹⁹ One important aspects of these compounds is the possibility to tune their

electrical properties by varying the cation content. In addition, in most of these compounds, two distinct elements can be introduced in the channels which contribute to add complexity and disorder in the structure and in some cases, result in polymorphism related to a different cluster arrangement.^{5,11-13,19} For instance, in the $\text{Ag}_x\text{Mo}_9\text{Se}_{11}$ compounds, increasing x from $x = 3.4$ up to $x = 3.9$ results in a progressive shift from metallic towards highly-doped semiconducting behavior.^{11,12} Upon substituting Ag by Tl or Rb,^{13,19} polymorph structures are obtained with distinct electronic properties. So far, ZT values varying between 0.4 and 0.7 have been achieved at 800 K in the $\text{Ag}_x\text{Mo}_9\text{Se}_{11}$ (for $x = 3.8$),^{11,12} $\text{Ag}_2\text{Tl}_2\text{Mo}_9\text{Se}_{11}$,¹³ $\text{Ag}_3\text{RbMo}_9\text{Se}_{11}$,¹⁹ and $\text{Ag}_3\text{In}_2\text{Mo}_{15}\text{Se}_{19}$ (Ref. 14) compounds.

In this last compound, the very low lattice thermal conductivity values ($0.4 \text{ W m}^{-1} \text{ K}^{-1}$ at 300 K) are equivalent to the amorphous limit showing that the phonon mean free path is near from its minimum possible value.¹⁴ However, the multiband nature of the electrical conduction is the main limiting factor that does not allow high thermopower values to be obtained. Due to its favorable thermal transport, higher thermoelectric performances could be expected if a single-carrier regime with optimal carrier concentration could be achieved. In an attempt to tune the electrical properties of this compound, we have considered the possibility to substitute In for Tl and successfully obtained phase-pure polycrystalline samples of the as-yet unreported Tl-filled cluster compound $\text{Ag}_3\text{Tl}_2\text{Mo}_{15}\text{Se}_{19}$.

Here, we present its synthesis, single-crystal structure and thermoelectric properties measured in the temperature range 5 – 800 K. The experimental results are complemented by theoretical calculations of the energy dependence of the density of states and of the temperature dependence of the electronic properties determined by a semi-classical approach using the Boltzmann transport equation. These combined theoretical and experimental results are further discussed in light of our prior study on the In analogue $\text{Ag}_3\text{In}_2\text{Mo}_{15}\text{Se}_{19}$.¹⁴

Experimental Section

Warning: Thallium and its compounds are toxic and must be handled with extreme care in a proper glove box environment.

Synthesis. Powders of Mo, MoSe₂, TlSe, and Ag (Strem, 99.95%) have been used as starting materials for the solid-state synthesis of Ag₃Tl₂Mo₁₅Se₁₉. The Mo powder (Plansee, 99.99%) was first treated under H₂ flowing gas at 1000°C during ten hours in order to eliminate traces of oxygen before the different syntheses. MoSe₂ was prepared by the reaction of selenium (Umicore, 99.999%) with H₂-reduced Mo in a ratio 2:1 in an evacuated (ca. 10⁻² Pa Ar residual pressure) silica tube, heated at 700°C during 48 h. TlSe was obtained directly from the metallic elements (Tl ingots, Strem Chemicals, 99.9%) heated at 500°C in evacuated silica tube during 48 h. All starting reagents were found monophasic based on their powder X-ray diffraction pattern collected on a D8 Bruker Advance diffractometer equipped with a LynxEye detector (CuKα₁ radiation). In order to avoid any contamination by oxygen and moisture, the starting reagents were kept and handled in a purified argon-filled glovebox.

Single-phase powders of Ag₃Tl₂Mo₁₅Se₁₉ were obtained by heating at 1300°C in a graphite resistance furnace (operating under about 0.8 bar argon pressure) during 40 h the required stoichiometric mixtures of Mo, Ag, TlSe, and MoSe₂ in molybdenum crucibles sealed under a low argon pressure (c.a. 0.6 bar argon pressure) using an arc welding system. The X-ray powder diffraction pattern of Ag₃Tl₂Mo₁₅Se₁₉ refined using the Rietveld method is shown in Figure 1. Refinement of the occupancy factor of the Ag and Tl atoms led to the values of 0.497(3) and 1.006(3), respectively, in very good agreement with the starting composition. Thus, no clear sub-stoichiometry in Ag or Tl is evidenced within the precision of these measurements. Crystallographic data and X-ray structural analysis for polycrystalline Ag₃Tl₂Mo₁₅Se₁₉ are summarized in Table S1 in the Supporting Information. The final atomic

coordinates and the equivalent isotropic displacement parameters are gathered in Table S2 in the Supporting Information, and selected interatomic distances are listed in Table S3 in the Supporting Information.

Single crystals were obtained by heating a cold-pressed pellet of $\text{Ag}_3\text{Tl}_2\text{Mo}_{15}\text{Se}_{19}$ powder in a molybdenum crucible at 1650 °C during 3h (the heating rates were 300°C/h and – 100°C/h for the warming and cooling ramps, respectively).

Hot Uniaxial Pressing (HUP). The obtained powders of $\text{Ag}_3\text{Tl}_2\text{Mo}_{15}\text{Se}_{19}$ were ground and subsequently densified by HUP sintering under a vacuum of about 10^{-2} mbar. Approximately 5 g of $\text{Ag}_3\text{Tl}_2\text{Mo}_{15}\text{Se}_{19}$ powder were introduced into a graphite matrix of \varnothing 12 mm previously coated with a thin boron nitride layer. The applied load was 50 MPa at the beginning of heating and was slowly increased up to 85 MPa to the sintering temperature of 1300 °C, which was maintained for 2 hours. The density of the pellet, obtained by measuring the volume and the weight, was about 98% of the theoretical density deduced from the crystallographic parameters.

Single Crystal Structure Determination. Intensity data were gathered on an Enraf-Nonius Kappa CCD goniometer (graphite-monochromatized MoK_α radiation, $\lambda = 0.71073\text{\AA}$) at 293 K. The COLLECT software²⁰ was used to determine the angular φ and ω scan conditions for the intensity collections. The intensity data sets were processed with the EvalCCD routine for the integration procedure.²¹ An analytical absorption correction following the de Meulenaer & Tompa algorithm was applied.²² The crystal structure was solved by isomorphism with $\text{Ag}_3\text{In}_2\text{Mo}_{15}\text{Se}_{19}$. Structure refinements and Fourier syntheses were performed using the JANA2006 package.²³ Similarly to the In cations in $\text{Ag}_3\text{In}_2\text{Mo}_{15}\text{Se}_{19}$, anisotropic displacement parameters of the Tl atoms were refined using an anharmonic approach based on a Gram-Charlier expansion²³ to better describe the electronic density around this cationic site, as shown by the difference-Fourier maps before (Figure 2a) and after the nonharmonic treatment

(Figure 2b). The anharmonic probability density function maps of Tl did not show any significant negative regions indicating that the refined model can be considered as valid.²⁴ Figure 3 shows the isosurface of the probability density for the Tl atoms. Refinement of the occupancy factor of the Ag site led to the final stoichiometry $\text{Ag}_{2.57}\text{Tl}_2\text{Mo}_{15}\text{Se}_{19}$. The sub-silver stoichiometry results from the higher temperature (1650 ° C) used during the crystal growth process which resulted in a loss of metallic silver, as confirmed by the formation of silver droplets on the lid of the molybdenum crucible. The crystal and structure refinement data for the $\text{Ag}_{2.57}\text{Tl}_2\text{Mo}_{15}\text{Se}_{19}$ compound are given in Table 1. The final fractional atomic coordinates as well as the equivalent isotropic displacement parameters and selected interatomic distances are listed in Tables 2 and 3, respectively.

Transport properties measurements. All the samples used for transport property measurements were cut with a diamond-wire saw from the consolidated cylindrical ingot with appropriate sizes and shapes. At low-temperatures (5 – 300 K), the electrical resistivity, thermopower and thermal conductivity were measured simultaneously using the thermal transport option (TTO) of a physical property measurement system (PPMS, Quantum Design). Copper bars utilized as thermal and electrical contacts were attached onto a bar-shaped sample ($\sim 1.5 \times 1.5 \times 8 \text{ mm}^3$) using a small amount of silver epoxy.

Hall effect measurements were performed with a five-probe configuration between 5 and 300 K under magnetic fields ranging between -1 and +1T using the ac transport option of the PPMS. Ohmic contacts were realized on the bar-shaped sample used for the TTO measurements by gluing copper wires onto the sample with a minute amount of conducting silver paste. The Hall resistivity ρ_H has been determined by measuring the antisymmetric component of the transverse ρ_{xy} voltage under magnetic field reversal following the formula

$\rho_H = [\rho_{xy}(+\mu_0 H) - \rho_{xy}(-\mu_0 H)]/2$. The linear-response Hall coefficient R_H was derived from

the slope of the $\rho_H(\mu_0 H)$ data for fields $\mu_0 H \leq 1\text{T}$. Because a nearly null signal was observed above 150 K, only data measured up to this temperature will be discussed.

Above room-temperature, a ZEM-3 apparatus (Ulva-Riko) was used to measure the electrical resistivity and thermopower simultaneously on bar-shaped samples ($\sim 1.5 \times 1.5 \times 8\text{ mm}^3$) cut perpendicularly to the pressing direction. This measurement was performed between 300 and 700 K by a conventional four-probe method under a low helium pressure. The thermal diffusivity a was measured on a circular pellet ($\sim 12\text{ mm}$ diameter, $\sim 1\text{ mm}$ thickness) between 300 and 700 K with a Netzsch laser flash instrument (LFA 467) under continuous argon flow. The sample was spray-coated with a thin layer of graphite prior to measurement to ensure a homogeneous signal absorption and emission on the respective surfaces. The measured thermal diffusivity was used to calculate the total thermal conductivity κ via the formula $\kappa = aC_p d$ where C_p is the specific heat and d is the experimental density. The density was deduced from the weight and the volume calculated from the geometric dimensions of the pellet. As a first approximation, C_p was estimated using the Dulong-Petit relation $C_p = 3NR$ where N is the number of atoms per formula unit and R is the gas constant. The temperature-dependence of the density was not taken into account in the present case.

Both longitudinal and transverse sound velocities were measured at 300 K on a disk-shaped sample using a pulse-echo method. A small quantity of honey was utilized to improve the coupling between the ultrasonic transducers and the sample.

Computational details. Density functional theory (DFT) calculations were performed using the WIEN2k program package.²⁵ The generalized gradient approximation (GGA) exchange-correlation functional within the parameterization of Perdew, Burke and Ernzerhof (PBE) was used for geometry optimizations.²⁶ A plane-wave cutoff of $R_{\text{MT}}K_{\text{max}} = 7$ was used while the radial wave-functions inside the non-overlapping muffin-tin spheres surrounding the atoms were expanded up to $l_{\text{max}} = 12$. The charge density was Fourier expanded up to the reciprocal

vector $G_{\max} = 14 \text{ \AA}^{-1}$. Total energy convergence was achieved with respect to the Brillouin zone (BZ) integration using a mesh of 500 k -points, generating 84 k -points in the irreducible BZ. Electronic dispersion curves and density of states (DOS) were shifted to set the Fermi level to 0 eV arbitrarily.

Electronic transport coefficients were calculated within the Boltzmann Transport Equation (BTE). A constant time relaxation τ for the electrons as well as a rigid band structure,^{27,28} as implemented in the BoltzTrap-1.2.5 code,²⁹ were assumed. 10 000 k -points in the BZ were used to compute the band derivatives and density of states for transport calculations.

Results and Discussion

Crystal Structure. The crystal structure of $\text{Ag}_{2.57}\text{Tl}_2\text{Mo}_{15}\text{Se}_{19}$ is shown in Figure 4. This compound is isostructural with $\text{Ag}_3\text{In}_2\text{Mo}_{15}\text{Se}_{19}$ ¹⁴ and consequently, its crystal structure is based on a mixture of $\text{Mo}_6\text{Se}_8^i\text{Se}_6^a$ and $\text{Mo}_9\text{Se}_{11}^i\text{Se}_6^a$ cluster units (cf. ref. 30, for explanations on the i - and a -type ligand notation) in equal proportions (Figure 5). The $\text{Mo}_6\text{Se}_8^i\text{Se}_6^a$ unit, the Mo core of which is the octahedral Mo_6 cluster, is similar to that seen in the Chevrel phases $M_x\text{Mo}_6\text{Se}_8$ for various cations M .⁴ The Mo_9 core of the second unit results from the face sharing of two octahedral Mo_6 clusters. The Mo_9 cluster is surrounded by 11 Se^i atoms capping the faces of the bioctahedron and 6 apical Se^a ligands above the ending Mo atoms. The center of the $\text{Mo}_6\text{Se}_8^i\text{Se}_6^a$ and $\text{Mo}_9\text{Se}_{11}^i\text{Se}_6^a$ cluster units correspond to a $6a$ (D_3 or 32 symmetry) and a $6b$ position (S_6 or $\bar{3}$ symmetry), respectively. In Table 3, we have summarized the main interatomic distances determined from refinements of the single-crystal X-ray diffraction data of $\text{Ag}_{2.57}\text{Tl}_2\text{Mo}_{15}\text{Se}_{19}$ and $\text{Ag}_3\text{In}_2\text{Mo}_{15}\text{Se}_{19}$ (Ref. 14) and from the Rietveld refinement against the PXRD data on $\text{Ag}_3\text{Tl}_2\text{Mo}_{15}\text{Se}_{19}$. In the following, only the

interatomic distances inferred from single-crystal X-ray diffraction will be discussed due to the higher precision achieved by this technique. The distances between the Mo1 atoms within the octahedral Mo₆ clusters are 2.6810 (4) Å for the intra-triangle distances (distances between Mo1 atoms related through the threefold axis) and 2.7098 (4) Å between the Mo1 atoms of two different adjacent triangles. The Mo-Mo distances in the bioctahedral Mo₉ clusters are 2.6466 (4) and 2.7235 (5) Å for the intra-triangle distances formed by the Mo2 and Mo3 atoms, respectively, and 2.6854 (2) and 2.7806 (2) Å for the distances between the (Mo1)₃ and (Mo2)₃ triangles. An examination of the different Mo-Mo distances observed in Ag_{2.57}Tl₂Mo₁₅Se₁₉ and Ag₃In₂Mo₁₅Se₁₉ (Table 3) shows that they only differ by at most 0.01 Å. The average Mo-Mo distances in the Mo₆ cluster are 2.695 and 2.690 Å for the Ag_{2.56}Tl₂Mo₁₅Se₁₉ and Ag₃In₂Mo₁₅Se₁₉ compounds, respectively, while in the Mo₉ cluster of the Tl and In compounds, these distances are equal to 2.707 and 2.706 Å, respectively. The slightly higher values observed in Ag_{2.57}Tl₂Mo₁₅Se₁₉ reflect the slight decrease in the number of electrons of the Mo₆ and Mo₉ clusters due to the deficiency in Ag. This fact is in agreement with electronic band structure calculations carried out using the LMTO method and has been previously observed when the cationic charge (that is, the In content x) decreases in the series In _{x} Mo₁₅S₁₉ ($0 \leq x \leq 3.7$).³¹ This last series of compounds is also based on Mo₆S₈ and Mo₉S₁₁ cluster units but arranged in a different way.

The Se1, Se2, Se4 and Se5 atoms bridge each one triangular faces of the clusters and the Se3 atom two triangular faces. In addition, the Se1 and Se2 atoms are linked to an external Mo atom of an adjacent cluster. The Mo-Se distances are comprised between 2.5672 (4) and 2.6274 (3) Å (average 2.594 Å) within the Mo₆Se₈ unit and between 2.5339 (3) and 2.7334 (3) Å within the Mo₉Se₁₁ unit (average 2.613 Å). Each Mo₉Se₁₁ (or Mo₆Se₈) entity is connected to six Mo₆Se₈ (or Mo₉Se₁₁) units via Mo1-Se2 bonds (or Mo2-Se1 bonds) to form the three-dimensional Mo-Se framework in which the shortest distance (Mo1-Mo2) between the Mo₆

and Mo₉ clusters is 3.5525 (3) Å thus leading to weak Mo-Mo interactions. The Tl⁺ ions are surrounded by 8 selenium atoms defining a distorted tetra-capped tetrahedron (Figure 6). The nearest four Se atoms, 3Se2 and Se5 forming the tetrahedron are at 3.2819(4) and 3.1579(9) Å, and the capping atoms (3Se1 and Se4) are at 3.6538(4) and 3.7235(9) Å, respectively. The silver atoms reside in distorted triangular-base bipyramidal sites located between two adjacent Tl sites with Ag-Se bond lengths comprised between 2.5630 (11) and 2.9326 (12) Å (Figure 6).

Electronic band structure. The electronic structures of several cluster-based molybdenum selenides have been studied using first-principles calculations.³² The electronic structure of compounds in which clusters are almost isolated from each other in the crystal structure can be deduced from the molecular orbital diagram of the isolated cluster unit. In the case of Ag₃In₂Mo₁₅Se₁₉, it has been shown that the metallic electron count (MEC), that is, the number of electrons available for metal-metal bonds, is equal to 57; whereas the optimal MEC is equal to 60. The former MEC corresponds to a monovalent character of indium and silver atoms, while the latter MEC is the sum of the optimal MEC of the Mo₆ and Mo₉ clusters that are equal to 24 and 36, respectively.¹⁴ The compound is expected to be semiconducting when the MEC reaches 60. The electronic band structure and density of states (DOS) of the model compound Ag₃Tl₂Mo₁₅Se₁₉ are shown in Figures 7 and 8. The DOS of the In-filled compound Ag₃In₂Mo₁₅Se₁₉ is also presented in Figure 8 for sake of comparison. The valence band is not completely filled by electrons suggesting a *p*-type metallic character. However, the band structure displayed in Figure 7 clearly shows that several bands near the Fermi level can contribute to the electrical conduction, suggesting that a more complex scheme can be observed in the transport properties of Ag₃Tl₂Mo₁₅Se₁₉ compared to Ag₃In₂Mo₁₅Se₁₉. The simultaneous presence of flat and dispersive bands near the Fermi level suggests that good

thermoelectric properties may be achieved since flat bands favors high thermopower while the dispersive character of the bands ensures high electrical conductivity.

Within a semi-classical approach, the electronic transport properties can be computed using the band structure. A previous theoretical study demonstrated that such an approach can help to predict the thermopower values of cluster compounds while it fails to qualitatively predict the electrical conductivity.³² The constant relaxation time approximation considered in such calculations is probably at the origin of this failure. The thermopower as a function of the chemical potential has been computed for $\text{Ag}_3\text{Tl}_2\text{Mo}_{15}\text{Se}_{19}$ and compared to that computed for the In analogue (Figure 9). Our calculations suggest that both compounds should exhibit similar thermopower values. Such a prediction is consistent with their similar crystal and electronic structures. However, the sharper DOS at the Fermi level in $\text{Ag}_3\text{In}_2\text{Mo}_{15}\text{Se}_{19}$ tends to favor larger effective mass (Fig. 7). Hence, the thermopower of this compound is expected to be slightly larger than that of the Tl analogue, assuming that both compounds possess similar carrier concentrations.

Electronic Transport Properties. Based on the above-mentioned MEC and electronic band structure, $\text{Ag}_3\text{Tl}_2\text{Mo}_{15}\text{Se}_{19}$ should behave as a heavily-doped semiconductor. The temperature dependences of the electrical resistivity and thermopower, shown in Figures 10a and 10b, confirm these predictions. Upon warming, the ρ values show a moderate decrease below 100 K before varying only slightly with temperature up to 800 K. The α values, positive over the entire temperature range, increase to reach a maximum value of $73 \mu\text{V K}^{-1}$ at 750 K. Both the *p*-type nature of the transport and the stronger metallic character of $\text{Ag}_3\text{Tl}_2\text{Mo}_{15}\text{Se}_{19}$ with respect to the In analogue (Ref. 14) are consistent with our calculations (*vide supra*). Although a slight Ag deficiency in polycrystalline samples may also explain these more pronounced metallic properties, our Rietveld refinements against the PXRD data did not evidence any clear sub-stoichiometry in neither of these elements. In addition, the deficiency

in Ag observed in single crystals is due to the very high temperature used during the crystal growth process. In contrast, the synthetic route used to prepare single-phase polycrystalline samples has been performed at lower temperatures, making a deviation in the Ag content from its nominal value unlikely in the polycrystalline samples. This conclusion is confirmed by the absence of Ag droplets observed either after synthesis or after HUP process. Despite $\text{Ag}_3\text{Tl}_2\text{Mo}_{15}\text{Se}_{19}$ exhibits lower α values with respect to $\text{Ag}_3\text{In}_2\text{Mo}_{15}\text{Se}_{19}$ as predicted by our calculations,¹⁴ the behavior of $\rho(T)$ over the whole temperature range is similar in both compounds. Since Hall effect measurements have evidenced a mixed electrical conduction in $\text{Ag}_3\text{In}_2\text{Mo}_{15}\text{Se}_{19}$,¹⁴ the similar $\rho(T)$ curves suggest that $\text{Ag}_3\text{Tl}_2\text{Mo}_{15}\text{Se}_{19}$ also features electron and hole pockets within the Brillouin zone.

This hypothesis is confirmed by the Hall data measured between 5 and 150 K (Figure 11a). Although the Hall coefficient R_H remains positive in this temperature range (Figure 11b) indicating dominant hole-like carriers, the measured values are strongly temperature-dependent. In contrast to the conventional expectation of a nearly temperature-independent Hall coefficient in heavily doped semiconductors, R_H decreases from $1 \times 10^{-2} \text{ cm}^3 \cdot \text{C}^{-1}$ at 5 K to $6.3 \times 10^{-3} \text{ cm}^3 \cdot \text{C}^{-1}$ at 150 K. Above this temperature, the signal is too small to be resolved by our measurement system. The most straightforward explanation of this behavior is that this strong variation in temperature arises from electron-like and hole-like charge carriers contributing to the Hall coefficient with their respective weights changing as a function of temperature. Above 150 K, both contributions almost compensate each other that explains the nearly null signal measured. A similar property has also been observed in $\text{Ag}_3\text{In}_2\text{Mo}_{15}\text{Se}_{19}$,¹⁴ for which a sign change in R_H has been evidenced near 25 K, as well as in other Mo-based cluster compounds.

Thermal Transport Properties. The total thermal conductivity is shown in Figure 12 as a function of temperature. Similarly to other Mo-based cluster compounds, κ exhibits a glass-

like temperature dependence with the absence of a dielectric maximum at low temperatures. κ increases monotonically to reach $1.5 \text{ W m}^{-1} \text{ K}^{-1}$ near 800 K. The lattice and electronic contributions to the thermal conductivity were disentangled using the Wiedemann-Franz relation ($\kappa_e = \dot{\iota} / \rho$) to estimate the latter. The Lorenz number L has been estimated assuming a single parabolic band model with acoustic phonon scattering as the main source of hole scattering. This simple approach led to L values that decrease from $2.45 \times 10^{-8} \text{ V}^2 \text{ K}^{-2}$ below 300 K, as expected for a degenerate hole gas, to $2.03 \times 10^{-8} \text{ V}^2 \text{ K}^{-2}$ at 800 K. The lattice thermal conductivity, obtained by subtracting κ_e from κ , is extremely low and comparable to other Mo-based cluster compounds (Figure 12). Above 300 K, κ_L approaches the minimum thermal conductivity κ_{min} estimated by the expression proposed by Cahill and Pohl³⁷

$$\kappa_{min} = \frac{1}{2} \left(\frac{\pi}{6} \right)^{1/3} \frac{k_B}{V^{2/3}} (2v_T + v_L)$$

where V is the average volume per atom, k_B is the Boltzmann constant and v_T and v_L are the transverse and longitudinal sound velocities, respectively. With $v_T = \dot{\iota} 1680 \text{ m s}^{-1}$ and $v_L = \dot{\iota} 3350 \text{ m s}^{-1}$, κ_{min} is equal to $0.38 \text{ W m}^{-1} \text{ K}^{-1}$.

Dimensionless thermoelectric figure of merit ZT . The combination of all thermoelectric properties leads to the temperature dependence of the calculated ZT values shown in Figure 13. The ZT values increases with increasing the temperature to reach a moderate peak value of 0.2 at 800 K. This maximum ZT is lower than that achieved in $\text{Ag}_3\text{In}_2\text{Mo}_{15}\text{Se}_{19}$ (Ref. 14) due to the lower thermopower values measured in $\text{Ag}_3\text{Tl}_2\text{Mo}_{15}\text{Se}_{19}$.

Summary and Conclusion

A new Tl-filled cluster compound based on Mo₆ and Mo₉ cluster units has been synthesized. Its crystal structure, determined by single-crystal X-ray diffraction, exhibits highly disordered Ag and Tl atoms distributed between the clusters units. According to electronic band structure calculations, this compound behaves as a heavily doped *p*-type semiconductor, a prediction confirmed experimentally by transport properties measurements. As in other Mo-based cluster compounds, the Hall signal is dominated by hole-like and electron-like contributions that explain the rather low thermopower values measured. The large inherent disorder due to the Ag and Tl atoms results in very low lattice thermal conductivity values that remain below 0.5 W.m⁻¹.K⁻¹ over the whole temperature range covered. The modest thermopower values is the main factor that limits the dimensionless thermoelectric figure of merit *ZT* to a maximum value of 0.2 at 800 K. The chemical flexibility of these cluster compounds to accommodate various elements between the cluster units offer nevertheless numerous possibilities to enhance their thermoelectric properties at high temperatures. The good correlation achieved between experiments and theoretical calculations makes the computations of the transport properties of these compounds a useful guidance for further experimental studies.

ASSOCIATED CONTENT

Supporting Information

The Supporting Information is available free of charge on the ACS Publications web site at.

Crystallographic data and X-ray structural analysis, final atomic coordinates and equivalent isotropic displacement parameters, and selected interatomic distances for polycrystalline Ag₃Tl₂Mo₁₅Se₁₉.

AUTHOR INFORMATION

Corresponding Authors

*E-mail: patrick.gougeon@univ-rennes1.fr (P. G.), alah1r@cmich.edu (R. A. R. A. O.)

ORCID

Patrick Gougeon: 0000-0003-4778-5581

Christophe Candolfi: 0000-0002-1248-5354

Notes

The authors declare no competing financial interest.

Acknowledgements

R. A. R. A. O. and B. B. are indebted to the Région Bretagne for a PhD grant.

Accepted manuscript

References

- (1) Goldsmid, H. J. in *Thermoelectric Refrigeration*; Springer: New York, 1964.
- (2) *Thermoelectrics and its Energy Harvesting*, ed. Rowe, D. M., CRC Press, 2012.
- (3) Bell, L. Cooling, Heating, Generating Power, and Recovering Waste Heat with Thermoelectric Systems. *Science* **2008**, *321*, 1457–1461.
- (4) Fischer; Ø. Chevrel Phases: Superconducting and Normal State Properties. *Appl. Phys.* **1978**, *16*, 1–28.
- (5) Gougeon, P.; Padiou, J.; Le Marouille, J.-Y.; Potel, M.; Sergent, M. $\text{Ag}_{3.6}\text{Mo}_9\text{Se}_{11}$ Premier Composé à Clusters Mo_9 dans des Motifs $\text{Mo}_9\text{Se}_{11}$. *J. Solid State Chem.* **1984**, *51*, 218–226.
- (6) Gougeon, P.; Potel, M.; Padiou, J.; Sergent, M. Synthesis, Crystal Structure and Electrical Properties of the First Compound Containing Uniquely $\text{Mo}_{12}\text{Se}_{14}$ Cluster Units. *Mat. Res. Bull.* **1987**, *22*, 1087–1092.
- (7) Gautier, R.; Picard, S.; Gougeon, P.; Potel, M. Synthesis, Crystal and Electronic Structures, and Electrical Properties of $\text{Rb}_2\text{Mo}_{12}\text{Se}_{14}$ Containing Trioctahedral Mo_{12} Clusters. *Mat. Res. Bull.* **1999**, *34*, 93–101.
- (8) a) Gougeon, P.; Potel, M.; Sergent, M. Structure of $\text{Rb}_3\text{Mo}_{15}\text{Se}_{17}$ Containing the New Mo_{15} Clusters. *Acta. Cryst.* **1989**, *C45*, 182–185.
- (9) Picard, S.; Saillard, J.-Y.; Gougeon, Noël, H. P.; Potel, M. $\text{Rb}_{2n}(\text{Mo}_9\text{S}_{11})(\text{Mo}_{6n}\text{S}_{6n+2})$ ($n = 1$ to 4): A Novel Family of Superconducting Molybdenum Cluster Compounds. *J. Solid State Chem.* **2000**, *155*, 417–426.
- (10) Picard, S.; Gougeon, P.; Potel, M. Single-Crystal Structure of $\text{Cs}_5\text{Mo}_{21}\text{S}_{23}$. *Acta. Cryst.* **1997**, *C53*, 1519–1521.

- (11) Zhou, T.; Lenoir, B.; Colin, M.; Dauscher, A.; Al Orabi, R. A. R.; Gougeon, P.; Potel, M.; Guilmeau, E. Promising Thermoelectric Properties in $\text{Ag}_x\text{Mo}_9\text{Se}_{11}$ Compounds ($3.4 \leq x \leq 3.9$). *Appl. Phys. Lett.* **2011**, *98*, No. 162106.
- (12) Zhou, T.; Colin, M.; Candolfi, C.; Boulanger, C.; Dauscher, A.; Santava, E.; Hejtmanek, J.; Baranek, P.; Al Rahal Al Orabi, R.; Potel, M.; Fontaine, B.; Gougeon, P.; Gautier, R.; Lenoir, B. Comprehensive Study of the Low-Temperature Transport and Thermodynamic Properties of the Cluster Compounds $\text{Ag}_x\text{Mo}_9\text{Se}_{11}$ ($3.41 \leq x \leq 3.78$). *Chem. Mater.* **2014**, *26*, 4765–4775.
- (13) Al Rahal Al Orabi, R.; Gougeon, P.; Gall, P.; Fontaine, B.; Gautier, R.; Colin, M.; Candolfi, C.; Dauscher, A.; Hejtmanek, J.; Malaman, B.; Lenoir, B. X-ray Characterization, Electronic Band Structure, and Thermoelectric Properties of the Cluster Compound $\text{Ag}_2\text{Tl}_2\text{Mo}_9\text{Se}_{11}$. *Inorg. Chem.* **2014**, *53*, 11699–11709.
- (14) Gougeon, P.; Gall, P.; Al Rahal Al Orabi, R.; Fontaine, B.; Gautier, R.; Potel, M.; Zhou, T.; Lenoir, B.; Colin, M.; Candolfi, C.; Dauscher, A. Synthesis, Crystal and Electronic Structures, and Thermoelectric Properties of the Novel Cluster Compound $\text{Ag}_3\text{In}_2\text{Mo}_{15}\text{Se}_{19}$. *Chem. Mater.* **2012**, *24*, 2899–2908.
- (15) Al Rahal Al Orabi, R.; Fontaine, B.; Gautier, R.; Gougeon, P.; Gall, P.; Bouyrie, Y.; Dauscher, A.; Candolfi, C.; Lenoir, B. Cu Insertion Into the Mo_{12} Cluster Compound $\text{Cs}_2\text{Mo}_{12}\text{Se}_{14}$: Synthesis, Crystal and Electronic Structures, and Physical Properties. *Inorg. Chem.* **2016**, *55*, 6616–6624.
- (16) Daigre, G.; Gougeon, P.; Gall, P.; Gautier, R.; Guillou, O.; Vaney, J.-B.; Candolfi, C.; Dauscher, A.; Lenoir, B. Synthesis, Crystal Structure and High-Temperature Transport Properties of the New Cluster Compound $\text{Rb}_2\text{Mo}_{15}\text{Se}_{19}$. *J. Solid State Chem.* **2016**, *237*, 1–6.
- (17) Masschelein, P.; Candolfi, C.; Dauscher, A.; Gendarme, C.; Al Rahal Al Orabi, R.; Gougeon, P.; Potel, M.; Gall, P.; Gautier, R.; Lenoir, B. Influence of S and Te substitutions on

the thermoelectric properties of the cluster compound $\text{Ag}_{3.8}\text{Mo}_9\text{Se}_{11}$. *Journal of Alloys and Compounds*, **2018**, 739, 360-367.

(18) Colin, M.; Zhou, T.; Lenoir, B.; Dauscher, A.; Al Rahal Al Orabi, R.; Gougeon, P.; Potel, M.; Baranek, P.; Semprimoschnig, C. Optimization of Bulk Thermoelectrics: Influence of Cu Insertion in $\text{Ag}_{3.6}\text{Mo}_9\text{Se}_{11}$. *J. Electron. Mater.* **2012**, 41, 1360–1364.

(19) Gougeon, P.; Gall, P.; Merdrignac-Conanec, O.; Aranda, L.; Dauscher, A.; Candolfi, C.; Lenoir, B. Synthesis, Crystal Structure, and Transport Properties of the Hexagonal Mo_9 Cluster Compound $\text{Ag}_3\text{RbMo}_9\text{Se}_{11}$. *Inorganic Chemistry*, **2017**, 56, 9684-9692.

(20) Nonius, B. V. COLLECT, data collection software; Nonius BV: Delft, The Netherlands, 1999.

(21) Duisenberg, A. J. M. Ph.D. Thesis, University of Utrecht, Utrecht, The Netherlands, 1998.

(22) de Meulenaer, J.; Tompa, H. The Absorption Correction in Crystal Structure Analysis. *Acta Crystallogr. Sect. A: Found. Crystallogr.* **1965**, 19, 1014–1018.

(23) Petricek, V.; Dusek, M. *Jana2006*; Institute of Physics, Academy of Sciences of the Czech Republic: Prague, Czech Republic, 2006.

(24) Johnson, C. K.; Levy, H. A. International Tables for X-ray Crystallography; Ibers, J. A., Hamilton, W. C., Eds.; Kynoch Press: Birmingham, U.K., 1974.

(25) Blaha, P.; Schwarz, K.; Madsen, G. K. H.; Kvasnicka, D.; Luitz, J. WIEN2k 14.2, Vienna, Austria (2011).

(26) Perdew, J. P.; Burke, K.; Ernzerhof, M. Generalized Gradient Approximation Made Simple. *Phys. Rev. Lett.* **1996**, 77, 3865–3868.

(27) Scheidemantel, T. J.; Ambrosch-Draxl, C.; Thonhauser, T.; Badding, J. V.; Sofo, J. O. Transport coefficients from first-principles calculations. *Phys. Rev. B* **2003**, 68, 125210.

- (28) Madsen, G. K. H. Automated Search for New Thermoelectric Materials: The Case of LiZnSb *J. Am. Chem. Soc.* **2006**, *128*, 12140–12146.
- (29) Madsen, G. K. H.; Singh, D. J. BoltzTrap. A Code for calculating band-structure dependent quantities. *Comput. Phys. Commun.* **2006**, *175*, 67–71.
- (30) Schäfer, H.; Von Schnering, H. G. Metall-Metall-Bindungen bei Niederen Halogeniden, Oxyden und Oxydhalogeniden Schwerer Übergangsmetalle Thermochemische und Strukturelle Prinzipien. *Angew. Chem.* **1964**, *20*, 833–849.
- (31) Salloum, D.; Gautier, R.; Gougeon, P.; Potel, M. Syntheses and Structural Trends of the $\text{In}_x\text{Mo}_{15}\text{S}_{19}$ ($0 \leq x \leq 3.7$) Compounds Containing Mo_6 and Mo_9 Clusters. *J. Solid State Chem.* **2004**, *177*, 1672–1680.
- (32) Al Rahal Al Orabi, R.; Boucher, B.; Fontaine, B.; Gall, P.; Candolfi, C.; Lenoir, B.; Gougeon, P.; Halet, J.-F.; Gautier, R. Towards the prediction of the transport properties of cluster-based molybdenum chalcogenides. *J. Mater. Chem. C.* **2017**, *5*, 12097–12104, and references therein.
- (33) Cahill, D. G.; Watson, S. K.; Pohl, R. O. Lower limit to the thermal conductivity of disordered crystals. *Phys. Rev. B: Condens. Matter Mater. Phys.* **1992**, *46*, 6131–6140.

Accepted manuscript

Figure Captions

Figure 1. Rietveld refinement of the PXRD pattern of $\text{Ag}_3\text{Tl}_2\text{Mo}_{15}\text{Se}_{19}$ ($R = 3.94$, $R_B = 5.86$, $R_p = 10.29$, $R_{wp} = 13.14$, $G.O.F = 1.45$). The red, black and blue lines show, respectively, the observed calculated and difference plots. The vertical blue ticks stand for the Bragg reflections.

Figure 2. Fourier difference maps in the (a, b) plane for $\text{Ag}_3\text{Tl}_2\text{Mo}_{15}\text{Se}_{19}$ before (a) and after (b) the nonharmonic refinement of the displacement parameters of the Tl atom (step: $0.2 \text{ e } \text{\AA}^{-3}$).

Figure 3. View along the c axis of the anharmonic probability density isosurface of Tl^+ . Se atoms are drawn at an arbitrary size. Level of the three-dimensional maps are at 0.01 \AA^{-3} .

Figure 4. Crystal structure of $\text{Ag}_3\text{Tl}_2\text{Mo}_{15}\text{Se}_{19}$ projected along the b -axis. The thermal ellipsoids are drawn at the 97% probability level.

Figure 5. Plot showing the atom-numbering scheme and the interunit linkage of the $\text{Mo}_6\text{Se}_8\text{Se}_6$ and $\text{Mo}_9\text{Se}_{11}\text{Se}_6$ units.

Figure 6. Selenium environments for the Tl and Ag atoms (ellipsoids are drawn at the 97 % probability level).

Figure 7. Electronic band structure of $\text{Ag}_3\text{Tl}_2\text{Mo}_{15}\text{Se}_{19}$ calculated by DFT.

Figure 8. Energy dependence of the density of states of $\text{Ag}_3M_2\text{Mo}_{15}\text{Se}_{19}$ ($M = \text{In}, \text{Tl}$).

Figure 9. Thermopower computed as a function of the chemical potential for $\text{Ag}_3M_2\text{Mo}_{15}\text{Se}_{19}$ with $M = \text{In}$ (plain) and Tl (dotted) at 300 K.

Figure 10. (a) Electrical resistivity ρ and (b) thermopower α as a function of temperature.

Figure 11. a) Transverse electrical resistivity ρ_{xy} as a function of the applied magnetic field $\mu_0 H$ measured at selected temperatures. b) Temperature dependence of the Hall coefficient R_H inferred from the field dependence of the Hall resistivity $\rho_H = [\rho_{xy}(+\mu_0 H) - \rho_{xy}(-\mu_0 H)]/2$.

Figure 12. Temperature dependence of the total thermal conductivity κ (red filled circles) and lattice thermal conductivity κ_L (blue filled squares). The horizontal solid black line stands for the estimated theoretical minimum of the thermal conductivity κ_{min} .

Figure 13. Dimensionless thermoelectric figure of merit ZT as a function of temperature.

Table 1. Crystal and Structure Refinement Data for $\text{Ag}_{2.57}\text{Tl}_2\text{Mo}_{15}\text{Se}_{19}$.

Formula	$\text{Ag}_{2.57}\text{Tl}_2\text{Mo}_{15}\text{Se}_{19}$
Formula weight ($\text{g}\cdot\text{mol}^{-1}$)	3616.6
Crystal system	trigonal
Space group	$R\bar{3}c$
a (\AA)	9.9601(1)
c (\AA)	57.3025(8)
Volume (\AA^3)	4923.02(10)
Z	6
ρ_{calc} ($\text{g}\cdot\text{cm}^{-3}$)	7.3193
Radiation, wavelength (\AA)	Mo $K\alpha$, 0.71073
Temperature of measurement (K)	293
θ_{max}	35°
Reflections collected/unique/ R_{int}	26285/2203/0.0567
Reflections with $I > 2\sigma(I)$	1806
Crystal dimensions (mm^3)	$0.237 \times 0.162 \times 0.111$
Absorption coefficient (mm^{-1})	37.647
Max/min transmission	0.1848/0.0243
Goodness-of-fit on F^2	1.14
R indices [$I > 2\sigma(I)$], R_1, wR_2	0.0223, 0.0468
R indices (all data), R_1, wR_2	0.0323, 0.0496
Largest diff. peak and hole	1.34, $-1.61 \text{ e}\cdot\text{\AA}^{-3}$

Table 2. Fractional atomic coordinates, equivalent isotropic displacement parameters (Å²), multiplicity, and site occupancy factors for Ag_{2.57}Tl₂Mo₁₅Se₁₉.

Atom	x	y	z	U _{eq}	Mult.	s.o.f
Ag	-0.24289(9)	-0.38211(12)	0.415203(19)	0.0335(5)	36	0.4274(12)
Tl	0	0	0.379670(12)	0.03513(12)	12	0.9829(18)
Mo1	-0.16293(3)	-0.14659(3)	0.480592(5)	0.00376(9)	36	1
Mo2	0.18576(3)	-0.32226(3)	0.455931(5)	0.00381(9)	36	1
Mo3	0.333333	-0.17546(4)	0.416667	0.00314(10)	18	1
Se1	-0.03449(4)	-0.31683(4)	0.482448(6)	0.00609(11)	36	1
Se2	-0.38088(4)	-0.36357(4)	0.454639(6)	0.00681(11)	36	1
Se3	0.03519(4)	-0.333333	0.416667	0.00660(13)	18	1
Se4	0	0	0.444650(9)	0.00848(13)	12	1
Se5	0.333333	-0.333333	0.491228(9)	0.00757(12)	12	1

Table 3. Main interatomic distances (Å) for $\text{Ag}_{2.57}\text{Tl}_2\text{Mo}_{15}\text{Se}_{19}$, $\text{Ag}_3\text{In}_2\text{Mo}_{15}\text{Se}_{19}$, and $\text{Ag}_3\text{Tl}_2\text{Mo}_{15}\text{Se}_{19}$.

	$\text{Ag}_3\text{Tl}_2\text{Mo}_{15}\text{Se}_{19}$ (Single crystal)	$\text{Ag}_3\text{In}_2\text{Mo}_{15}\text{Se}_{19}^{14}$ (Single crystal)	$\text{Ag}_3\text{Tl}_2\text{Mo}_{15}\text{Se}_{19}$ (Powder)
Ag-Se2	2.6988(12)	2.726(3)	2.680(11)
Ag-Se2	2.6443(13)	2.677(3)	2.725(11)
Ag-Se3	2.5630(11)	2.5885(9)	2.549(7)
Ag-Se4	2.9326(12)	2.881(2)	2.973(9)
Tl/In-Se1 (x3)	3.6538(4)	3.5815(6)	3.635(3)
Tl/In-Se2 (x3)	3.2819(4)	3.2806(4)	3.289(3)
Tl/In-Se4	3.7235(9)		3.745(5)
Tl/In-Se5	3.1579(9)	2.9893(12)	3.101(5)
Mo1-Mo1 (x2)	2.6810(4)	2.6784(3)	2.681(3)
Mo1-Mo1 (x2)	2.7098(5)	2.7007(2)	2.714(3)
Mo1-Mo2	3.5527(5)	3.5694(4)	3.555(4)
Mo1-Se1	2.5869(6)	2.5854(3)	2.583(3)
Mo1-Se1	2.6122(6)	2.6173(4)	2.612(5)
Mo1-Se1	2.5672(4)	2.5726(3)	2.603(3)
Mo1-Se2	2.6274(4)	2.6340(4)	2.621(3)
Mo1-Se4	2.5764(5)	2.5812(4)	2.588(4)
Mo2-Mo2 (x2)	2.6466(6)	2.6455(2)	2.652(4)
Mo2-Mo3	2.6854(3)	2.6820(2)	2.694(2)
Mo2-Mo3	2.7806(4)	2.7763(2)	2.786(3)
Mo2-Se1	2.6912(5)	2.6947(3)	2.681(4)
Mo2-Se2	2.6435(5)	2.6538(5)	2.649(4)
Mo2-Se2	2.5695(4)	2.5675(4)	2.561(4)
Mo2-Se3	2.6754(4)	2.6699(2)	2.680(3)
Mo2-Se5	2.5349(5)	2.5339(4)	2.540(4)
Mo3-Mo3 (x2)	2.7235(4)	2.7334(4)	2.749(4)
Mo3-Se2 (x2)	2.6139(4)	2.6265(3)	2.628(3)

Mo3-Se3 (x2)	2.5732(4)	2.5729(3)	2.581(3)

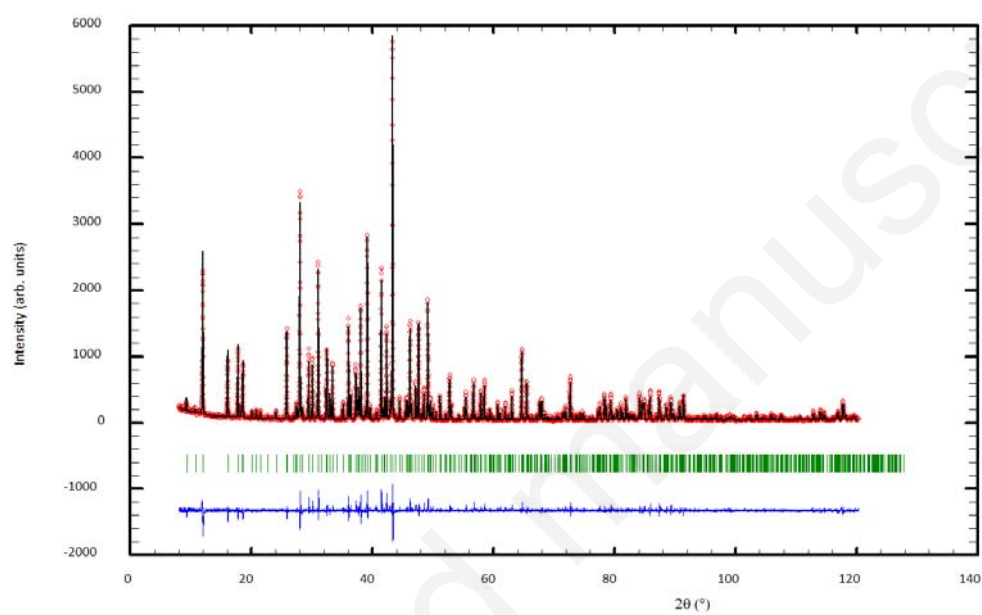
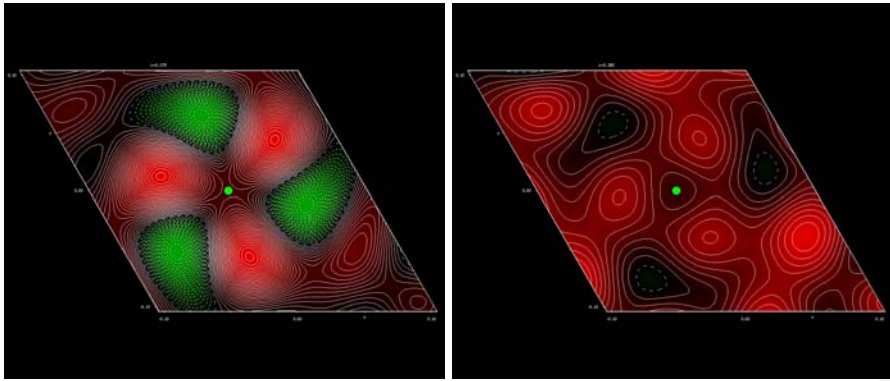


Figure 1

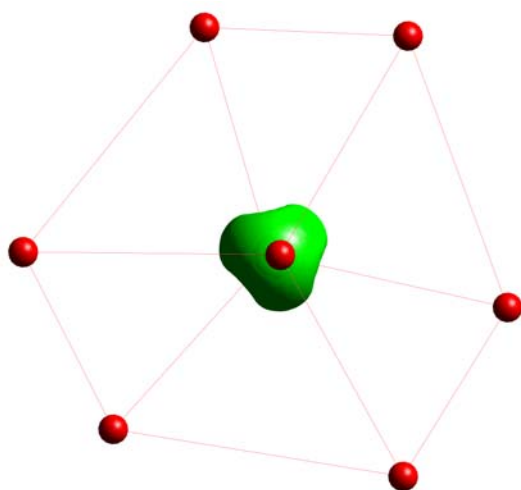


(a)

(b)

Figure 2

Accepted manuscript



Accepted manuscript

Figure 3

Accepted manuscript

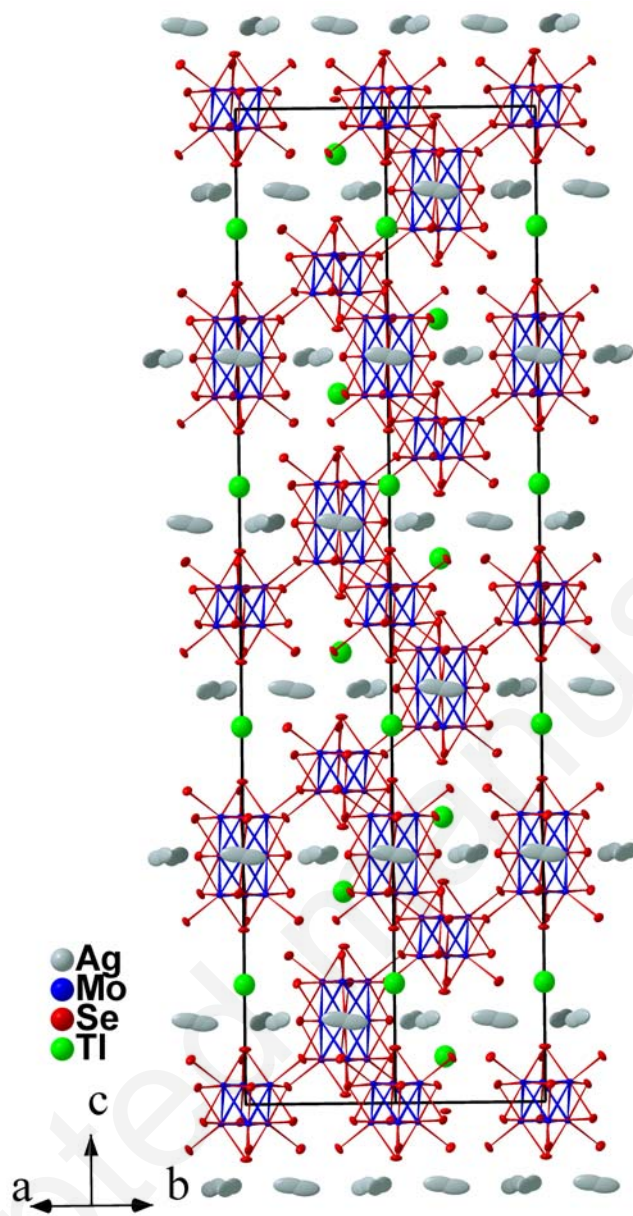


Figure 4

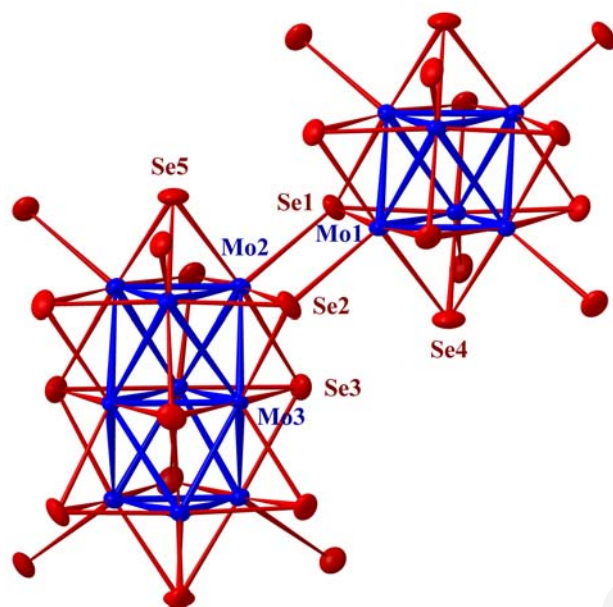


Figure 5

Accepted manuscript

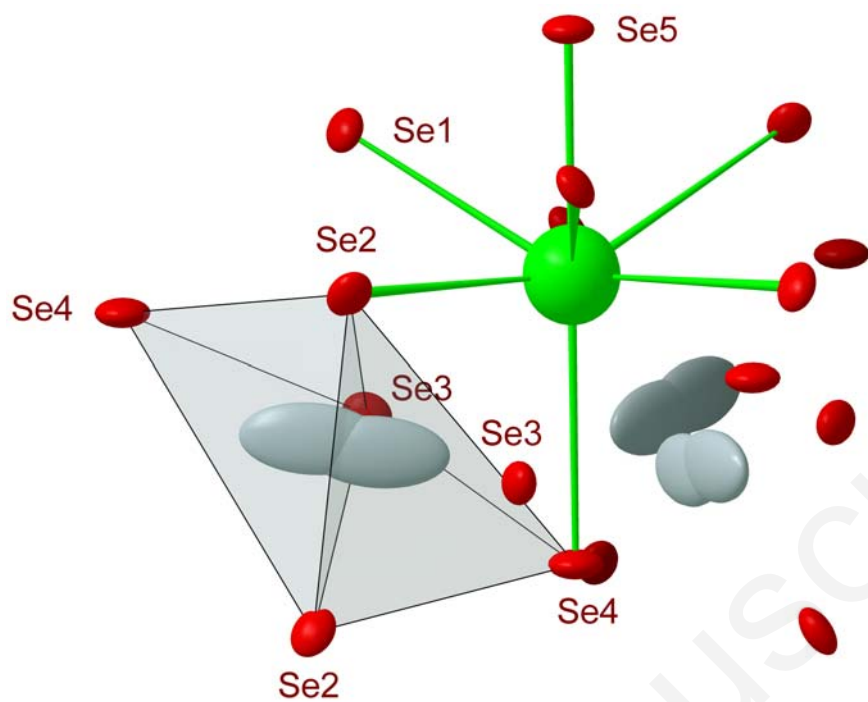


Figure 6

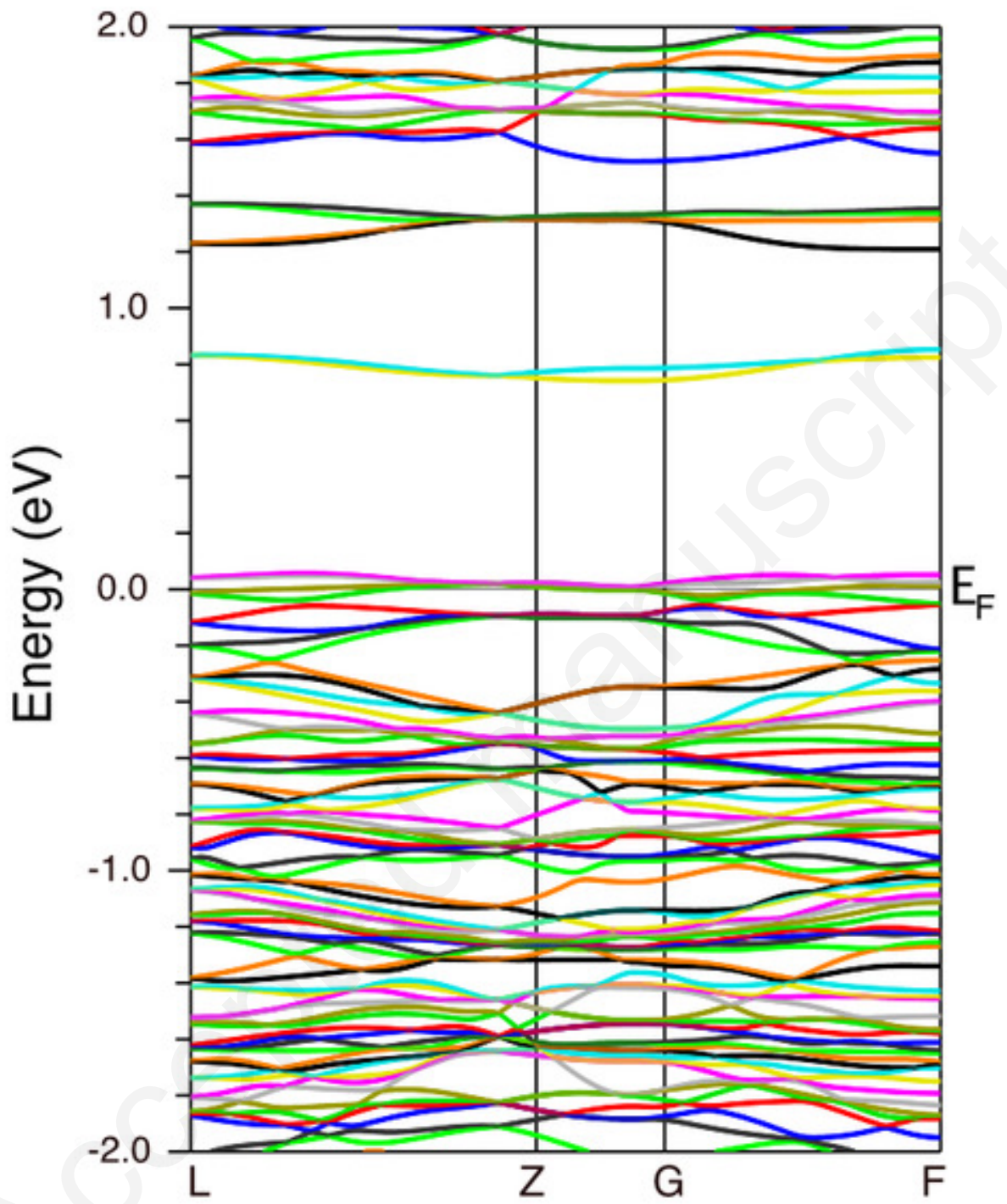


Figure 7

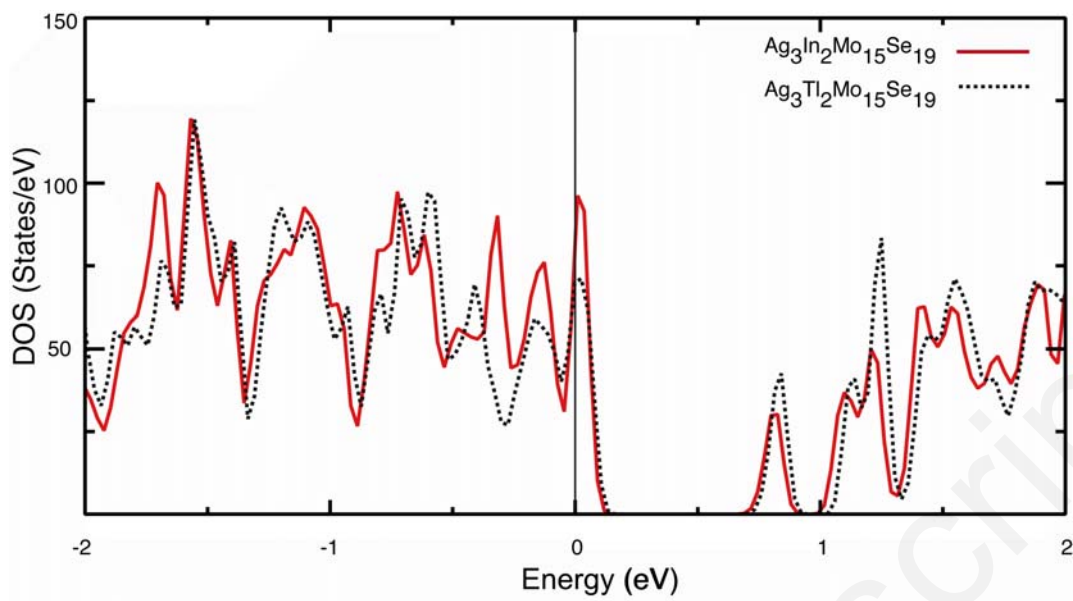


Figure 8

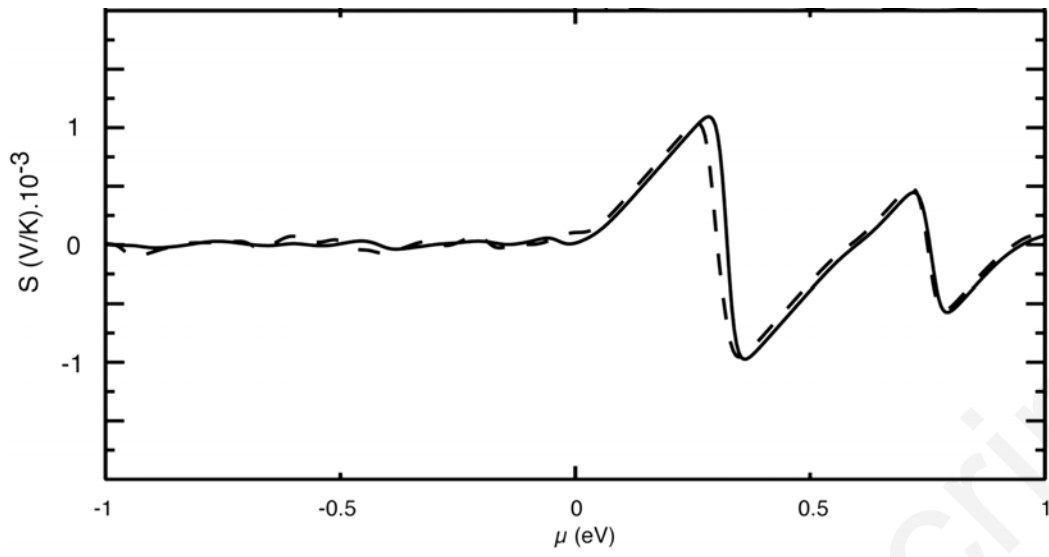


Figure 9

Accepted manuscript

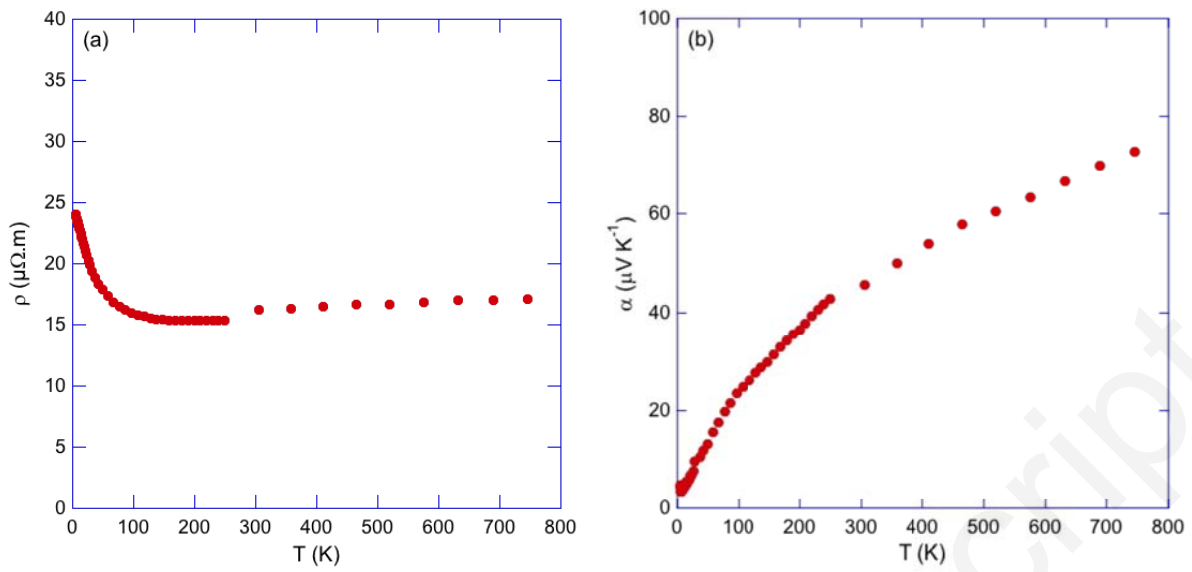


Figure 10

Accepted manuscript

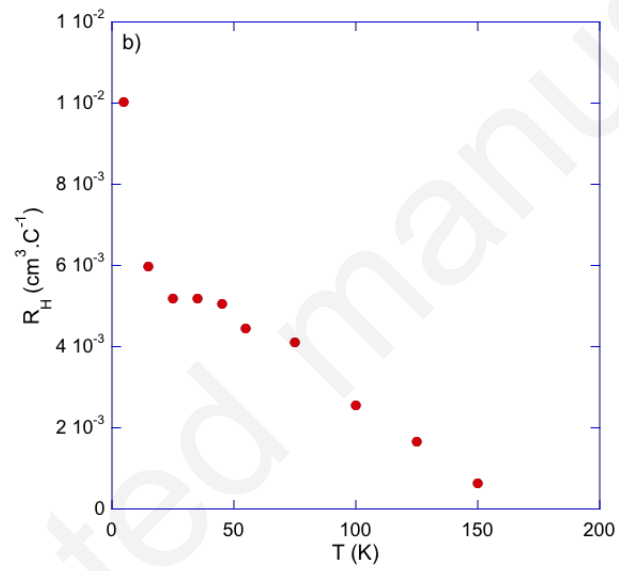
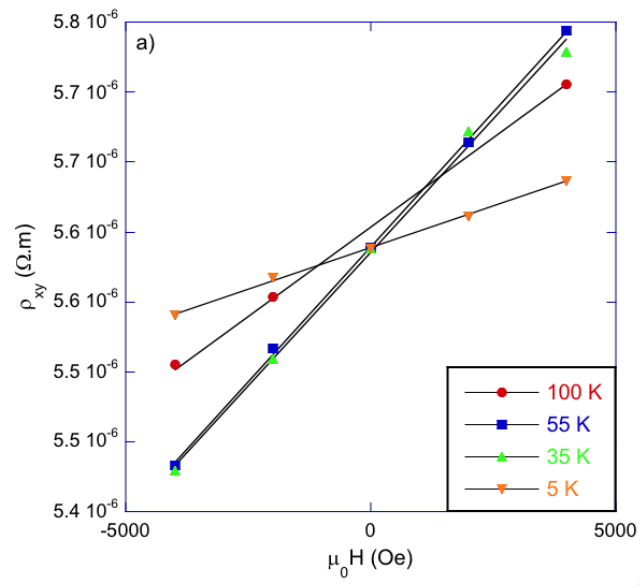


Figure 11

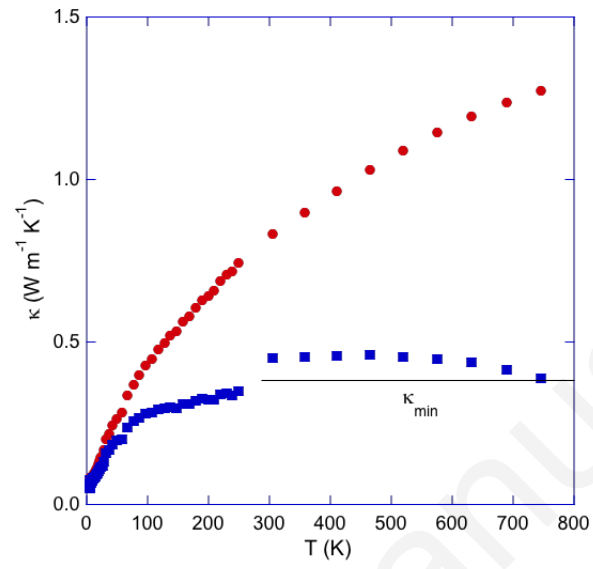


Figure 12

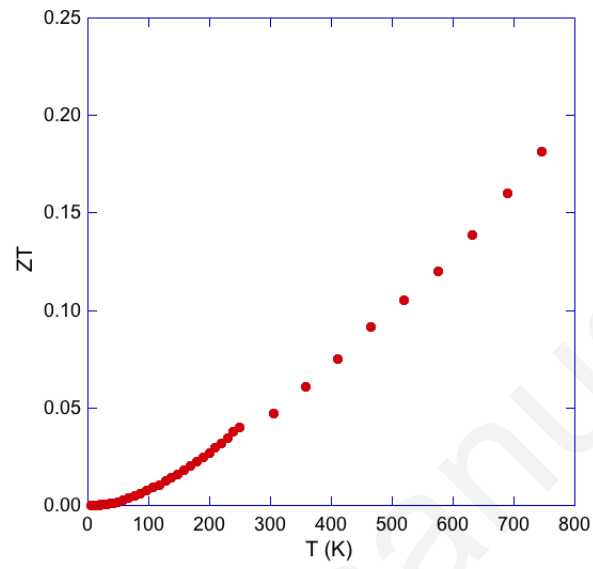


Figure 13

For Table of Contents Only

$\text{Ag}_3\text{Tl}_2\text{Mo}_{15}\text{Se}_{19}$ constitutes an Ag-filled variant of $\text{Tl}_2\text{Mo}_{15}\text{Se}_{19}$ containing Mo_6 and Mo_9 clusters. Its metallic behavior is in agreement with electronic band structure calculations carried out using the LMTO method. The complex unit cell together with the cage-like structure of $\text{Ag}_3\text{Tl}_2\text{Mo}_{15}\text{Se}_{19}$ results in very low thermal conductivity values leading to a ZT of 0.2 at 1100 K.

